# Rugged, obstruction-free, mirror–lens combination for panoramic imaging

W. Stürzl,[1,2,*] D. Soccol,[2,3] J. Zeil,[2] N. Boeddeker,[1,2] and M. V. Srinivasan[2,3]

[1]Department of Neurobiology and Center of Excellence "Cognitive Interaction Technology," Bielefeld University, P.O. Box 100131, 33501 Bielefeld, Germany

[2]Australian Research Council Centre of Excellence in Vision Science and Centre for Visual Sciences, Research School of Biological Sciences, The Australian National University, P.O. Box 475, Canberra, ACT 2601, Australia

[3]Visual and Sensory Neuroscience, Queensland Brain Institute, The University of Queensland, QBI Building (79), St. Lucia, QLD 4072, Australia

*Corresponding author: wolfgang.stuerzl@uni-bielefeld.de

Received 30 July 2008; accepted 22 September 2008; posted 2 October 2008 (Doc. ID 99584); published 6 November 2008

We present a new combination of lenses and reflective surfaces for obstruction-free wide-angle imaging. The panoramic imaging system consists of a reflective surface machined into solid Perspex, which together with an embedded lens, can be attached to a video camera lens. Unlike vision sensors with a single mirror mounted in front of a camera, the view in the forward direction (i.e., the direction of the optical axis) is not obstructed. Light rays contributing to the central region of the image are refracted at a centrally positioned lens and at the Perspex enclosure. For the outer image region, rays are reflected at a mirror surface of constant angular gain machined into the Perspex and coated with silver. The design produces a field of view of approximately 260° with only a small separation of viewpoints. The shape of the enclosing Perspex is specifically designed in order to minimize internal reflections. 

*OCIS codes:* 080.0080, 110.0110, 150.0150.

## 1. Introduction

Panoramic imaging devices with reflective surfaces are widely used in robotics [1–5], surveillance [6–8], and biological research [9–11]. However, most designs suffer from two problems: inadequate field of view and obstructions from holding arrangements that are needed to support and keep the reflective surfaces aligned with the optical axis of the camera. In addition, the reflective surfaces need to be protected from dust and mechanical damage. This is typically achieved by encasing the camera and reflective surface in a glass or Perspex cylinder, which, however, introduces distortions and spurious reflections, especially outdoors.

Here we describe a novel catadioptric imaging system, i.e., a mirror–lens combination that avoids these problems in addition to being rugged. We first give an overview of the system (Section 2), derive the shape of the Perspex block from which it is made (Section 3), and discuss the location of viewpoints of the imaging system (Section 4). In Section 5 we provide information about the manufacturing and polishing of the optical surfaces. Section 6 explains the unwarping and stitching of an omnidirectional image, and Section 7 discusses the imaging properties of the uncoated Perspex without additional lens. Finally Section 8 analyses possible issues regarding camera focus.

## 2. Design Overview

An overview of the new imaging system is shown in Fig. 1. It consists of an almost spherical solid

0003-6935/08/326070-09$15.00/0

Perspex block with a specially designed curved shape. The Perspex block is mounted directly on to an off-the-shelf camera lens via a short cylindrical Perspex column opposite the mirror surface. The internal reflective surface is coated with a thin silver layer on the outside and is shaped in such a way that it generates an image with a constant vertical angular gain [12,13]. The apex of this reflective surface is left uncoated. The resulting image is thus divided into two parts (see also example camera image in Section 6). The central part of the image is formed by refraction first at a plano-concave lens (focal length $f = -12\,\mathrm{mm}$), then at the uncoated curved surface, and finally at the planar surface before entering the camera lens. For the outer, panoramic part of the image, those incoming light rays that will reach the camera lens pass through the outer air–Perspex interface orthogonal to the almost spherical surface (see Section 3) before they are reflected at the inner reflective surface and refracted at the planar surface.

The shape of the reflective surface is given by (see Fig. 2(a) and [12])

$$\mathbf{x}(\eta) := r(\eta)\begin{pmatrix}\sin\eta\\ \cos\eta\end{pmatrix}, \qquad \eta \in (0, \eta_{\max}), \tag{1}$$

$$r(\eta) := r_0 \frac{\cos^k \gamma}{\cos(\eta/k + \gamma)^k}, \qquad k := \frac{2}{1+\alpha}, \tag{2}$$

where $\eta$ is the angle between the incoming rays and the optical axis, parametrizing the curve, $r_0$ is the distance from the nodal point of camera to the apex, $\gamma$ is the tangent angle at the apex of the mirror surface, $\eta_{\max}$ is the maximum angle covered by the reflective surface, and $\alpha$ is the vertical angular gain. The parameter values for the imaging device shown in Fig. 1 are $r_0 = 65\,\mathrm{mm}$, $\gamma = 0°$, $\eta_{\max} = 12°$, and $\alpha = 13$. The refraction at the planar camera-facing Perspex surface (with refractive index $n_p \approx 1.5$) causes the effective viewpoint of the camera to be shifted downward by $\Delta d \approx d(n_p - 1) \approx 10\,\mathrm{mm}$, where $d = 20\,\mathrm{mm}$ is the distance of the nodal point of the camera from the planar surface [see Fig. 3(a)]. In addition, the overall gain is reduced by a factor $n_p^{-1} \approx 2/3$, yielding an effective overall gain of $\alpha_{\mathrm{eff}} = n_p^{-1}\alpha \approx 8.7$. These approximations are valid for small angle $\eta$ for which the law of refraction is $\eta \approx n_p \eta_p$ ($\eta_p$ is the angle of the ray with respect to the surface normal within the Perspex block). The exact shift of the viewpoint depends on $\eta$, $\Delta d = d(1 - \tan\eta/\tan(\arcsin(n_p^{-1}\sin\eta)))$, and the angular gain is reduced by $\arcsin(n_p^{-1}\sin\eta)/\eta$. The almost spherical shape of the Perspex enclosure is derived in Section. 3.

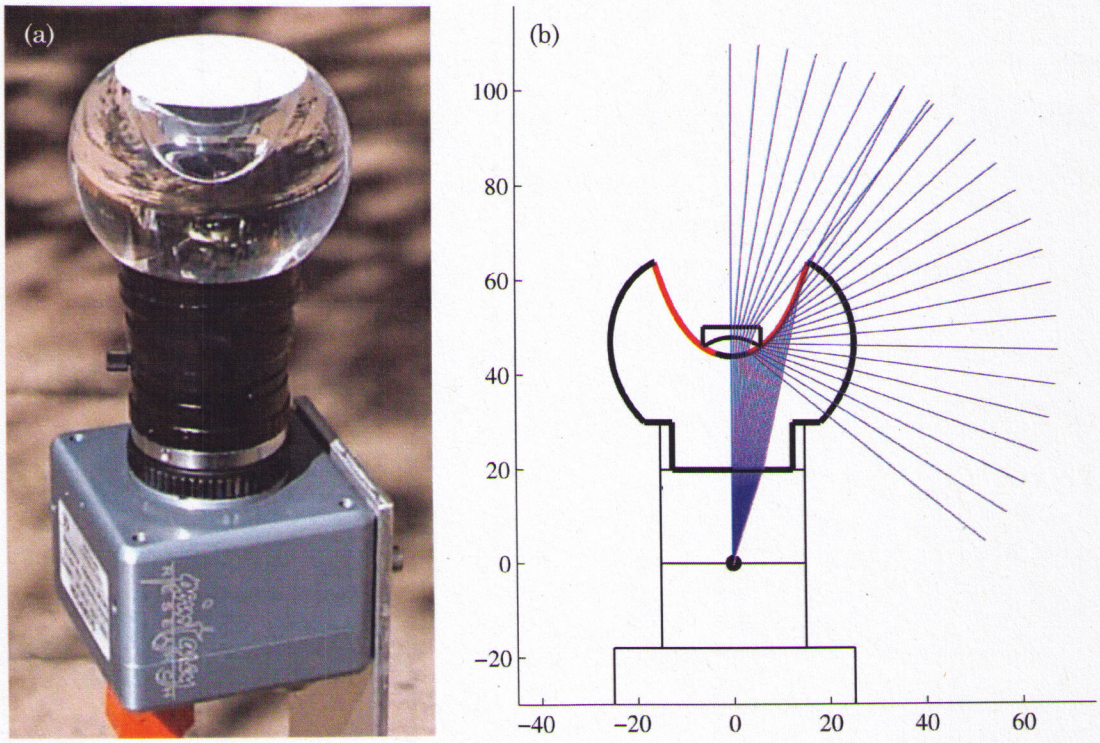


Fig. 1. (Color online) Overview of the new panoramic imager. (a) Picture showing the imaging arrangement mounted on a firewire video camera (1/2" CCD sensor) with an off-the-shelf 6 mm C-mount lens. The Perspex block can be attached to the filter thread of the camera lens. (b) Vertical transect and ray tracing for the new sensor. The surface of the clear Perspex is shown as a bold curve. The red curve shows where the Perspex is coated with a thin reflective surface. Through a central hole in the coating, rays are refracted at the curved surface of the Perspex and by a plano-concave lens.

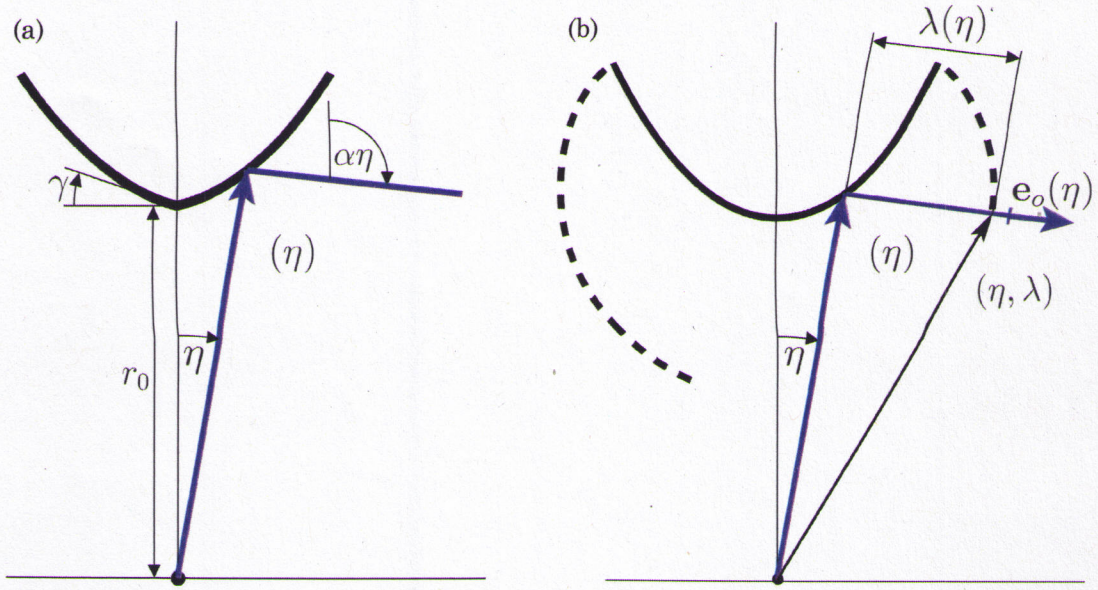


Fig. 2. (Color online) (a) Reflective surface with constant vertical angular gain and the parameters used in Eqs. (1) and (2). (b) Illustration of the parameters used in the derivation of the outer Perspex shape (Section 3).

For directions of view close to the optical axis of the camera, where the image is formed by refraction only, the angular gain lies between 6.8 and 8.2. However, since the angular gains are similar for the outer and the central parts of the image, it is easy to create an unwarped image with uniform constant gain in elevation by pixel resampling (see Section 6).

Because of the design, a slight difference in viewpoints for the outer and central parts of the image is necessary in order to achieve a complete coverage of the forward field of view. Otherwise a small occlusion would need to be tolerated.

### A. Related Work

While most previous approaches to panoramic imaging use a single convex mirror mounted in front of a camera lens, see [14] for an overview, there is a commercially available product that looks, at first glance, similar to our imager. However, this system, called PAL (panoramic annular lens), works quite differently. It uses a combination of concave and convex reflective surfaces and covers a smaller elevation range (see [15]).

## 3. Shape of Perspex Block

To minimize internal reflections and to preserve the constant gain property of the reflective surface, it is important to ensure that outgoing reflected rays hit the outer Perspex–air interface perpendicular to the local tangent plane as shown in Fig. 3 (to calculate the angular mapping, it is usually easier to examine outgoing rays emanating from the nodal point of the camera).

Since the reflective surface is a constant gain surface, defined by Eq. (1), the reflected rays are described by [see Fig. 2(b)]

$$\mathbf{f}(\eta, \lambda) := \mathbf{x}(\eta) + \lambda \mathbf{e}_o(\eta), \qquad \lambda \in \mathcal{R}^+, \tag{3}$$

$$\mathbf{e}_o(\eta) := \begin{pmatrix} \sin(\alpha\eta + 2\gamma) \\ -\cos(\alpha\eta + 2\gamma) \end{pmatrix}, \tag{4}$$

where $\mathbf{x}(\eta)$ is a point on the reflective surface, $\mathbf{e}_o(\eta)$ is a unit vector describing the direction of an outgoing ray, and $\lambda$ is a scalar that gives the distance from the reflective surface as measured along the direction of the reflected ray.

To calculate the surface, we need to find $\lambda(\eta)$ so that

$$\frac{\mathrm{d}\mathbf{f}(\eta, \lambda)}{\mathrm{d}\eta} \mathbf{e}_o(\eta) = 0, \tag{5}$$

i.e., the reflected rays hit the outer surface of the Perspex block orthogonally. This surface is then given by

$$\mathbf{F}(\eta) := \mathbf{f}(\eta, \lambda(\eta)). \tag{6}$$

Simplifying

$$\frac{\mathrm{d}\mathbf{f}}{\mathrm{d}\eta} \mathbf{e}_o = \left( \frac{\partial \mathbf{x}}{\partial \eta} + \lambda \frac{\partial \mathbf{e}_o}{\partial \eta} + \mathbf{e}_o \frac{\partial \lambda}{\partial \eta} \right) \mathbf{e}_o, \tag{7}$$

$$= \mathbf{x}' \mathbf{e}_o + \lambda \frac{\partial \mathbf{e}_o}{\partial \eta} \mathbf{e}_o + \frac{\partial \lambda}{\partial \eta} \mathbf{e}_o^2, \tag{8}$$

using $(\partial \mathbf{e}_o / \partial \eta) \mathbf{e}_o = 0$ and $\mathbf{e}_o^2 = 1$, Eq. (5) becomes

$$\frac{\partial \lambda}{\partial \eta} = -\frac{\partial \mathbf{x}}{\partial \eta}\mathbf{e}_o. \tag{9}$$

From Eq. (1) we find

$$\frac{\partial \mathbf{x}(\eta)}{\partial \eta} = \frac{\partial r(\eta)}{\partial \eta}\begin{pmatrix}\sin\eta\\ \cos\eta\end{pmatrix} + r(\eta)\begin{pmatrix}\cos\eta\\ -\sin\eta\end{pmatrix}, \tag{10}$$

$$\frac{\partial r(\eta)}{\partial \eta} = r_0\frac{\sin(\eta/k+\gamma)}{\cos(\eta/k+\gamma)^{(k+1)}} = r(\eta)\frac{\sin(\eta/k+\gamma)}{\cos(\eta/k+\gamma)}. \tag{11}$$

Using Eqs. (4), (10), and (11) and some algebraic manipulation, we obtain from Eq. (9)

$$\frac{\partial \lambda(\eta)}{\partial \eta} = -\frac{\partial r(\eta)}{\partial \eta}. \tag{12}$$

Integrating Eq. (12) with regard to $\eta$, we find

$$\lambda(\eta) = -r(\eta) + c_0, \tag{13}$$

where $c_0$ is a constant of integration to be determined by boundary conditions. Hence the shape of the outer surface, Eq. (6), is given by

$$\mathbf{F}(\eta) = \mathbf{x}(\eta) + (c_0 - r(\eta))\mathbf{e}_o(\eta). \tag{14}$$

If the outer surface of the Perspex block is to touch the mirror at $\mathbf{x}(\eta_{\max})$ [as in Fig. 3(a)], i.e., $\mathbf{F}(\eta) = \mathbf{x}(\eta_{\max})$, we have $c_0 = r(\eta_{\max})$.

Using a similar approach, "orthogonal Perspex surfaces" for other reflective surfaces can be calculated. For single viewpoint mirrors [16], for instance, for a hyperbolic mirror or a parabolic mirror with a telecentric camera lens, the orthogonal surface is simply a sphere.

### A. Real Image Created by Perspex Block

Since the refractive index of Perspex ($n_p \approx 1.5$) is different from the refractive index of air, the Perspex block itself acts as a lens. Figure 4 shows an example of a real image that is created close to the surface of the Perspex block. However, this image will only be seen by the camera if a bright object is closer than approximately 2 cm from the Perspex block.

## 4. Viewpoints

In a lens–mirror combination like the one we present here, it is important to achieve a near-constant viewpoint to aid the subsequent reassembly of different image parts (see Section 6). This is particularly important when viewing very close objects.

In the central part of our device, outgoing rays intersect almost exactly at a single point located at approximately (0, 42.5 cm) [see Fig. 3(b)]. This is not the case, however, for rays reflected at the constant gain surface, where viewpoints lie on a caustic surface [17]. As derived in [18], the cross-section of this surface is described by the curve

$$\mathbf{c}(\eta) = r(\eta)\left[\begin{pmatrix}\sin\eta\\ \cos\eta\end{pmatrix} - \frac{1}{\alpha}\begin{pmatrix}\sin(\alpha\eta+2\gamma)\\ -\cos(\alpha\eta+2\gamma)\end{pmatrix}\right], \tag{15}$$

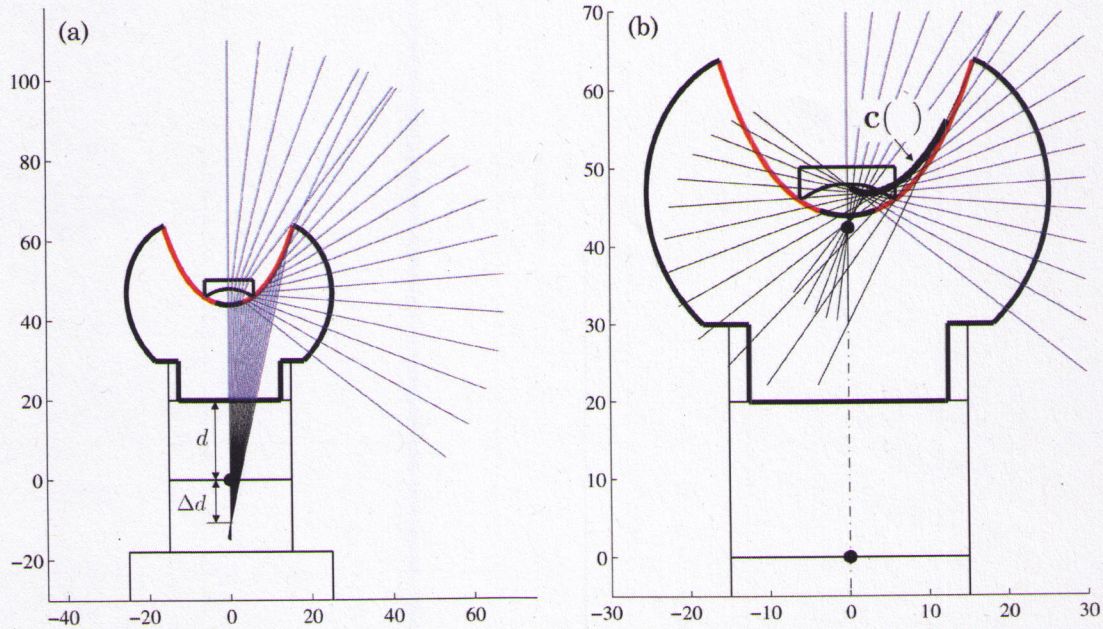


Fig. 3. (Color online) (a) Shape of the air–Perspex interface of the Perspex block is calculated so that rays hit the surface orthogonally. Because of the refraction at the planar surface, the effective viewpoint of the camera lens with respect to the reflective surface is at $(0, -\Delta d) \approx (0, -10\,\text{mm})$ ($d = 20\,\text{mm}$ is the distance of the nodal point from the planar surface). (b) Effective viewpoints of the sensor (see Section 4). The black dot at (0, 42.5 mm) marks the location of the approximate single viewpoint of the central/frontal field. The black curve shows the caustic of effective viewpoints $\mathbf{c}(\eta)$ for the reflected rays, defined in Eq. (15).

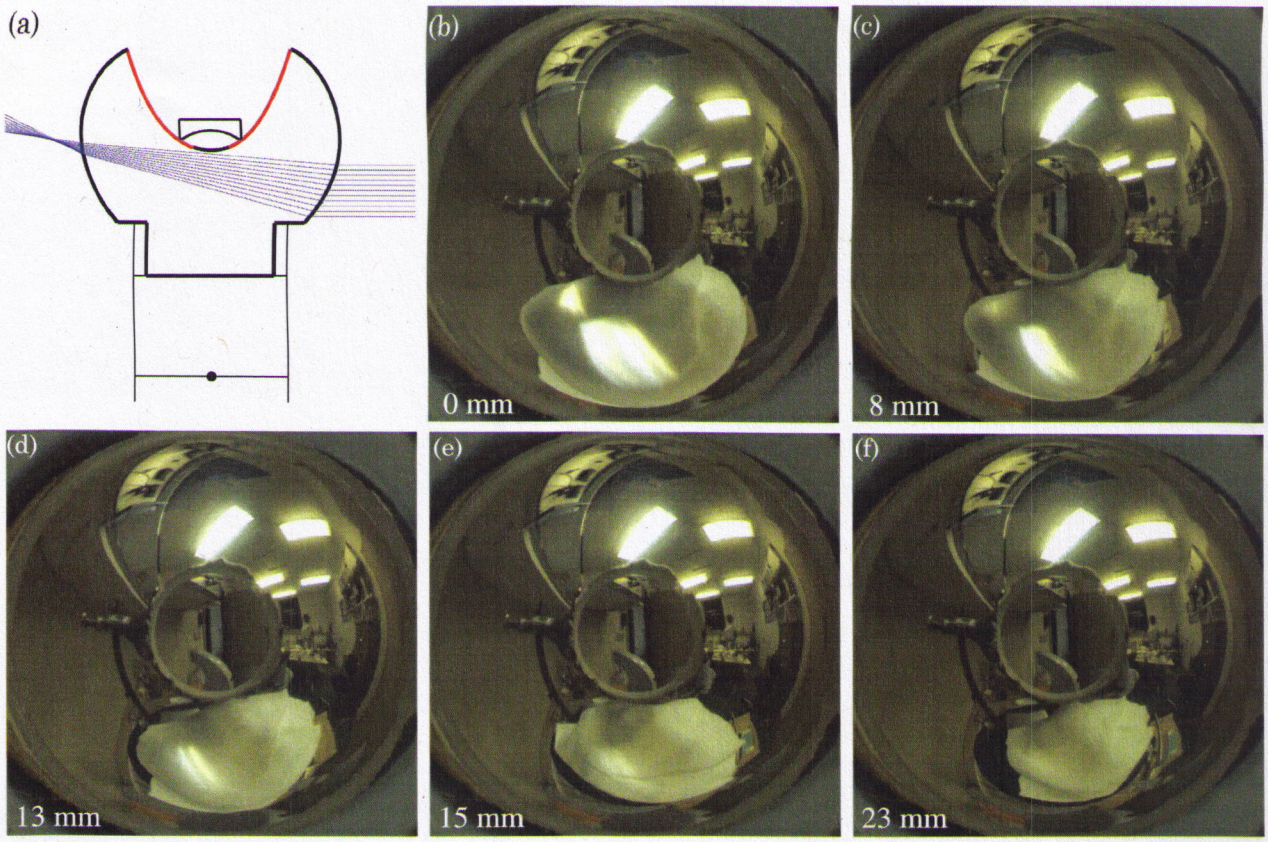


Fig. 4. (Color online) Real image created by the Perspex block. (a) Ray tracing for a vertical transect. (b)–(f) Real image of a ceiling light made visible by holding a white cloth close to the Perspex (bottom part of images). The values in the lower left corner give the approximate distances of the cloth to the Perspex. The imaging device is mounted with its optical axis oriented horizontally.

where $\gamma = 0$ and $\alpha = 13$ for our imaging device. The caustic is shown as a thick black curve in Fig. 3(b).

Corresponding to the discontinuity between the central and outer parts of the image, there is also a small discontinuity in viewpoints. However, the perpendicular distance of all reflected rays from the viewpoint of the central image never exceeds 5.5 mm.

### 5. Manufacture of the New Panoramic Imager

After machining the Perspex shape, the mirror surface and the outer surface of the Perspex block were polished. Polishing was done first with fine dry and wet sandpaper then with metal polish. The finish was done with silver polish. The apex of the future reflective surface (central part of the curved surface) was covered with a small bolt and the outer surface of the Perspex block with masking tape [see Fig. 5(b)] before the surface was silver coated by vacuum deposition. The thin silver layer was protected with white spray paint. After removing the masking tape and the bolt, the plano-concave lens was glued into place.

### 6. Unwarping and Stitching of an Omnidirectional Image

Figure 6 shows how an omnidirectional image covering −40° to +90° in elevation is assembled using the central and the outer part of the camera image. After mapping both image parts to spherical coordinates (unwarping), image blending is applied to the small overlapping region to achieve a smooth transition.

The omnidirectional image mapped to a sphere is shown in Fig. 7. Depending on the illumination and exposure time, it may become impossible to keep the whole camera image in perfect focus due to the varying optimal depth of focus of the reflective surface (see Section 8). The best compromise for focus setting is to tolerate slight blur in the outermost part of the image, because this part is mapped into a comparatively small solid angle on the viewing sphere.

### 7. Uncoated Surface—Refraction and Total Internal Reflection

It is interesting to investigate how the Perspex block performs without the silver coating and the lens. Since the Perspex has a higher refraction index ($n_p \approx 1.5$) than air ($n \approx 1$), total internal reflection will occur for angles of reflection

$$\phi \geq \phi_{\min} = \arcsin(n_p^{-1}) \approx 41.8°. \tag{16}$$

For a constant gain surface of gain $\alpha$, the colatitude $\theta$ (see Fig. 8) depends on the angle of reflection according to

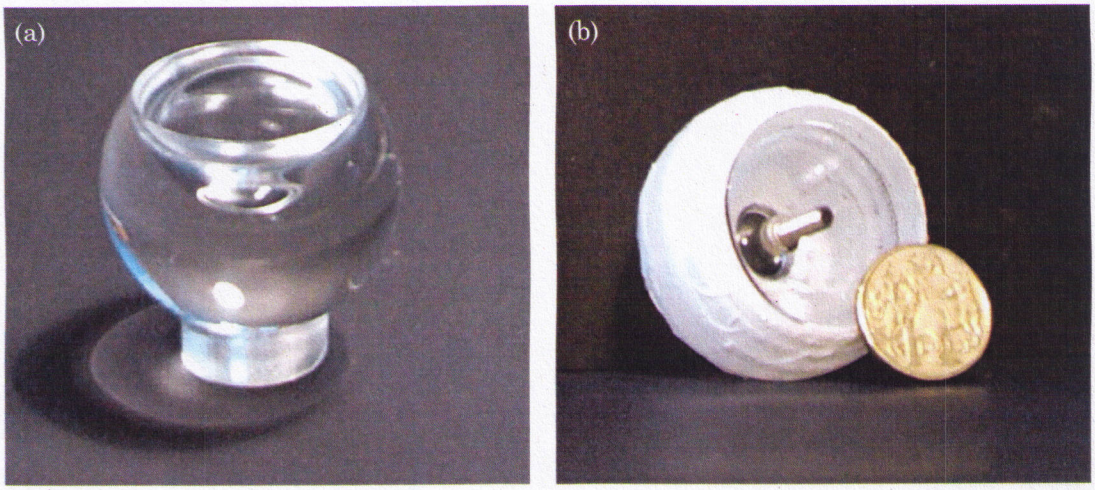


Fig. 5. (Color online) (a) Polished, solid Perspex block. (b) Masking tape and small bolt for masking the outer surface and the central part during vacuum deposition (an earlier version with an exactly spherical shape of the Perspex block is shown).

$$\theta = 180° - \frac{2\alpha}{\alpha + 1}\phi. \tag{17}$$

Thus the maximum colatitude for which total internal reflection occurs is

$$\theta_{\max} = 180° - \frac{2\alpha}{\alpha + 1}\arcsin(n_p^{-1}). \tag{18}$$

For the manufactured shape with $\alpha = 13$, we have $\theta_{\max} \approx 102.4°$. Since the central part covers the region of the scene that is not imaged by reflection, the total field of view of the uncoated Perspex is approximately 200° (see Fig. 9). Compared to conventional wide-angle lenses (that typically have a field of view $\lesssim$180°), the advantage of this mirror–lens combination lies in the fact that imaging the horizon is made easy. However, the angular gain in the image center is much smaller than for the outer image part that is formed by total internal reflection at the constant gain shape. There is thus a fovea-like central image part with angular gain of approximately 3–5, compared to $\alpha \approx 2/3 \times 13 \approx 8.7$ for the reflective surface.

Compared to the setup with coating and lens, the effective viewpoints for the refracted and reflected rays at the discontinuity lie slightly closer together [see Fig. 9(a) and compare with Fig. 3). However, the overlap of central and outer image parts is smaller, and focusing problems may become an

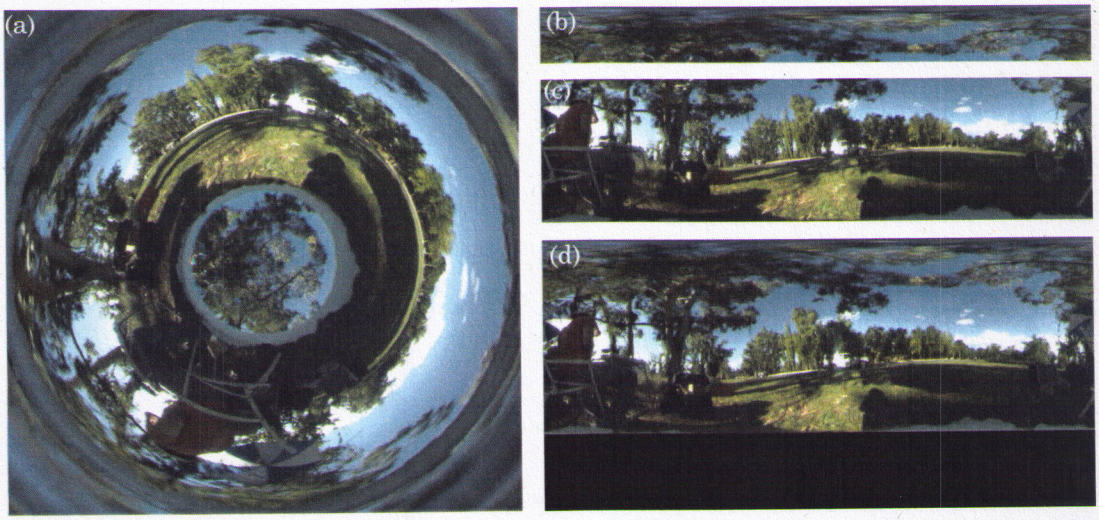


Fig. 6. (Color online) (a) Camera image of an outdoor scene with the imaging device pointing upward toward the sky. The gray regions at the border between the central and the outer part of the image are caused by damage to the reflective layer at that location. (b) Unwarped central image region. (c) Unwarped outer/panoramic image region. (d) Stitched omnidirectional image covering the whole sphere, azimuth $\in (-180°, 180°)$, elevation $\in (-90°, 90°)$. The black area shows the elevation range $(-90°, -40°)$ not imaged by the vision sensor. Note that the camera was not levelled.

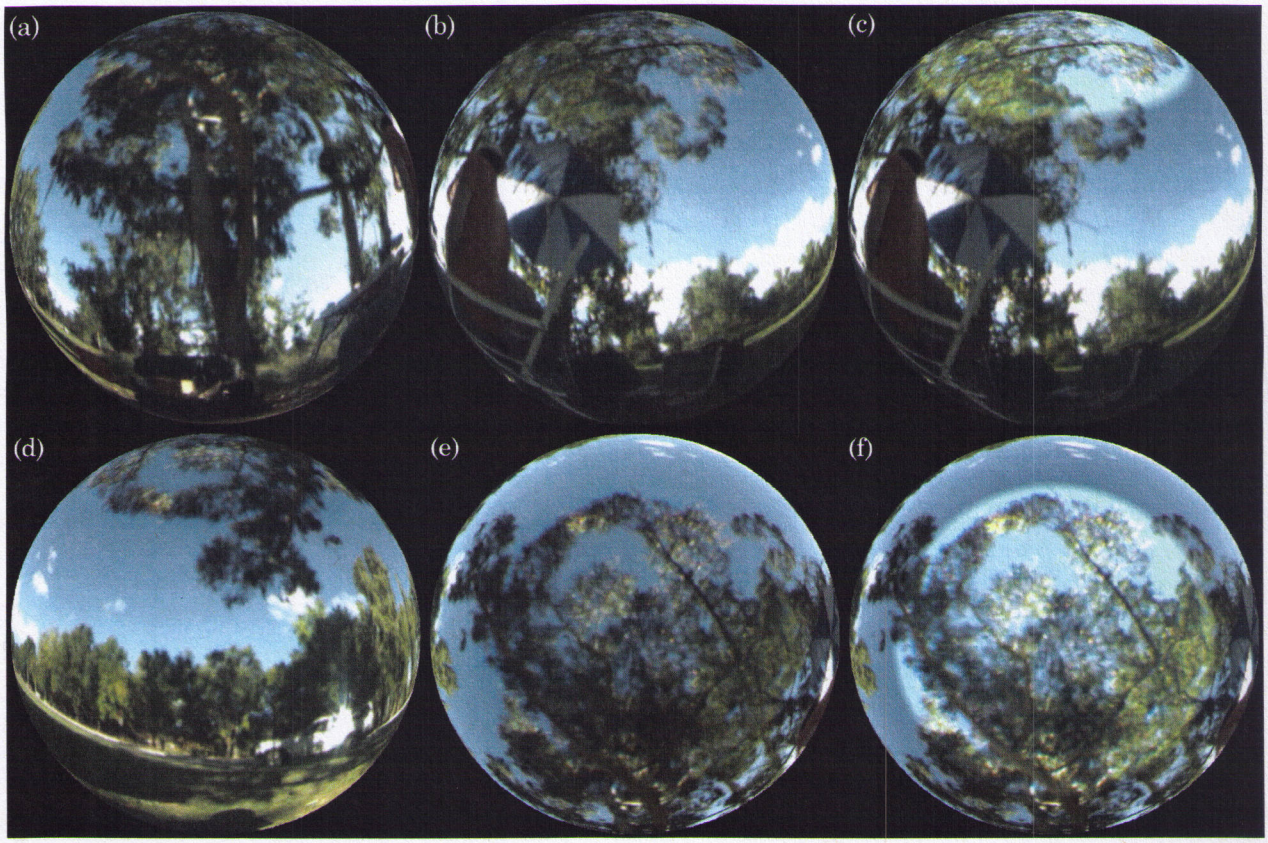


Fig. 7. (Color online) Omnidirectional image of Fig. 6(d) mapped to a sphere. Different viewing directions are shown. In (c) and (f), the remapped central image part is highlighted.

issue because the optimal camera lens focus is now farther away for the central part of the image [see Fig. 10(b)].

Figures 9(c) and 9(d) show examples of camera images for the uncoated version. The images were taken with an earlier version where the enclosing surface is spherical [see Fig. 9(b)]. The two parts of the image are separated by a narrow annulus in which refracted rays are reflected from the inner side of the constant gain surface.

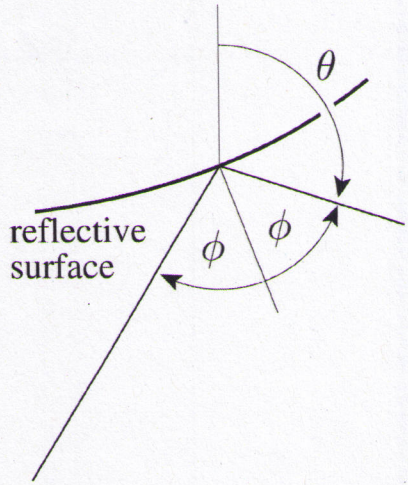


Fig. 8. Reflection angle $\phi$ and colatitude $\theta$.

## 8. Camera Focus and Image Blur

This section discusses the problem of focus and blur for the central and outer image regions. To estimate the virtual image created by the reflective surface, we applied the theoretical framework described in [18], taking into account the refraction at the air–Perspex interfaces. This approach considers vertically and horizontally shifted parallel light rays to estimate the location of caustic surfaces (shown as dashed and solid blue curves in Fig. 10).

For the central part, we discuss the simplest case of the virtual image for incident rays, namely, rays parallel to the optical axis. The intersection point of the back-projected refracted rays gives the position of the virtual image. From Fig. 10(a) we see that this point lies within the range of the virtual images created by the reflective surface. Thus focusing close to the virtual image of the central image region also results in a reasonably well-focused image of the outer region. The dashed curve starts close to the solid curve, but distance between the curves increases farther away from the optical axis. Thus a good focus in all parts of the outer image is hard to achieve in low-light conditions. However, since large elevation

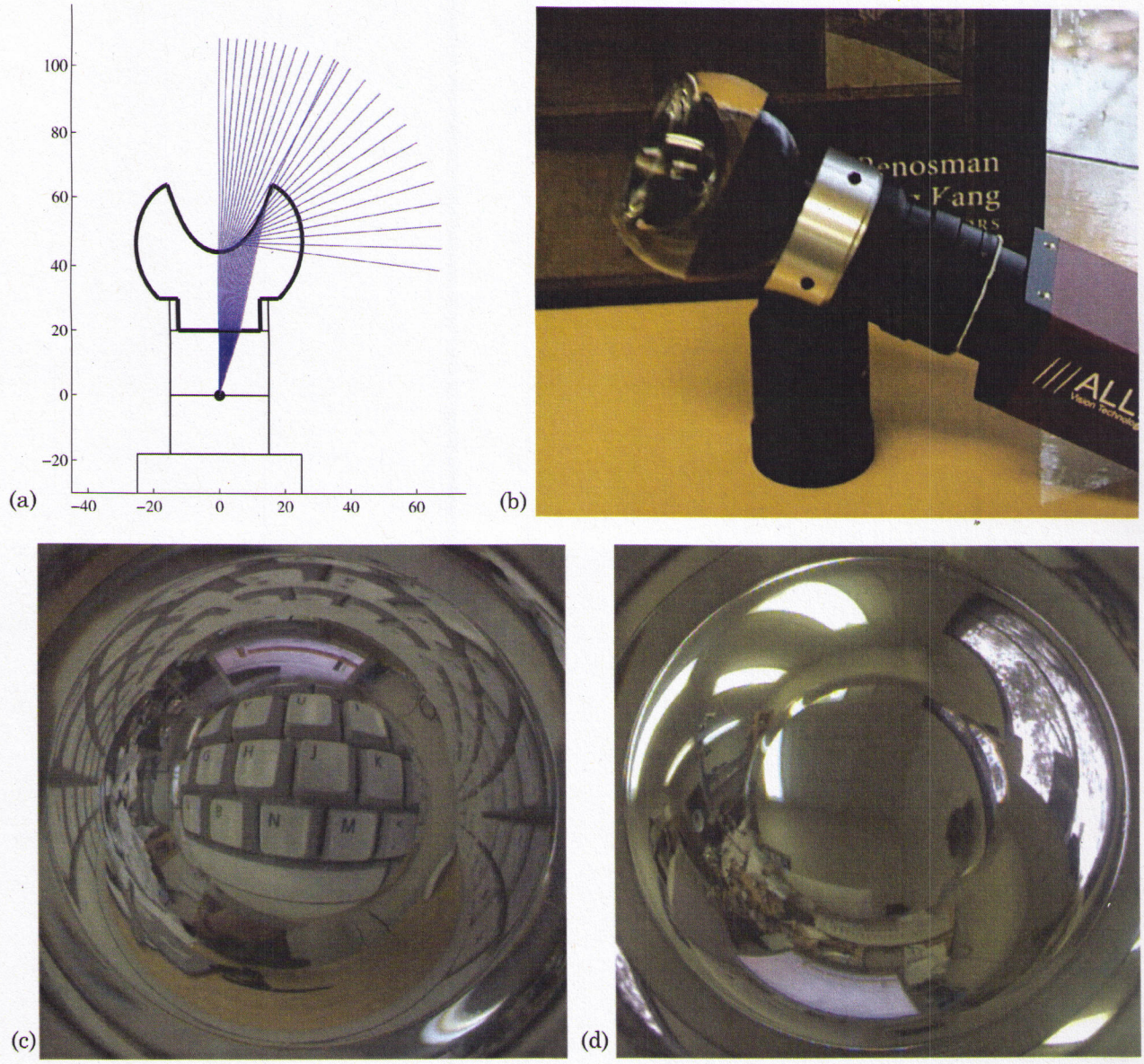


Fig. 9. (Color online) Imaging properties of the uncoated Perspex. (a) Ray tracing diagram showing the refraction of the rays in the image center and total internal reflection in the outer part of the image. (b) Setup used to test the uncoated sensor. An earlier version of the vision sensor with exact spherical shape was used. The part of the sphere that does not contribute to the image is covered with black tape to eliminate unwanted internal reflections. (c) Camera image showing the total internal reflection (camera oriented toward a computer keyboard). (d) Image that shows the small overlap between central and outer image parts more clearly. Note the part of window frame that is imaged twice on the right side.

angles, which correspond to small solid angles on the unit sphere, are mapped to large circles in the camera image, slight blur along circles is acceptable in the outer image part. The effect of this blur is greatly reduced when the image is mapped onto a sphere (see Section 6).

Figure 10(b) shows the estimated virtual image at the optical axis for an uncoated Perspex block. It is farther away from the solid blue curve and thus can lead to more image blur (see also Section 7).

Naturally the severity of the effects we have described depends heavily on the camera lens aperture and will be less pronounced in outdoor applications and in bright light when the aperture can be stopped down.

## 9. Conclusions

We have presented a novel catadioptric imaging system consisting of a reflective surface machined into a solid Perspex block of a specific profile, carrying an embedded lens. Since the device can be manufactured quite easily, it is well suited for applications that require a low-cost, wide-angle, obstruction-free, rugged imaging system. The Perspex imager has

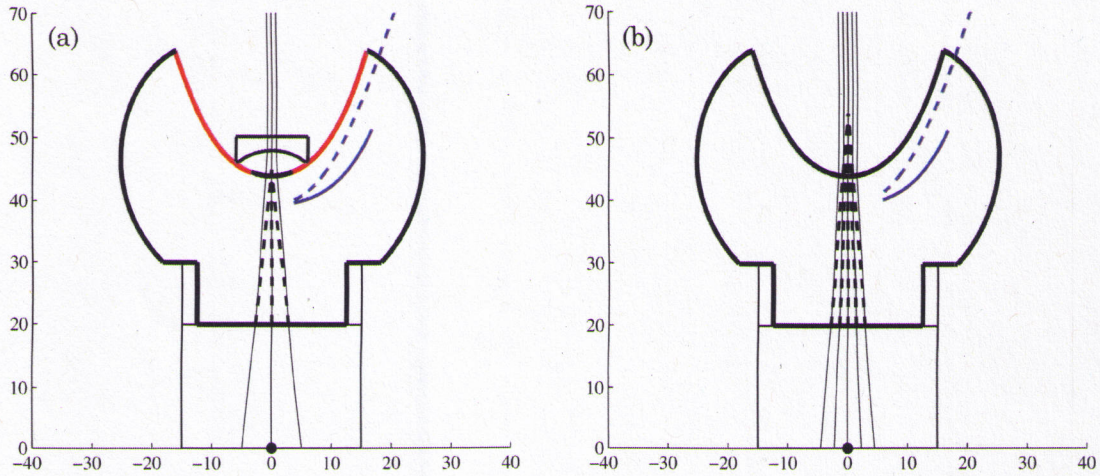


Fig. 10. (Color online) Locations of virtual images. The blue curves in the right-hand side of the figures show the virtual images created by the reflective surface (solid: for vertically shifted rays; dashed: for horizontally shifted rays). The intersection of the black dashed rays gives the location of the virtual image at the optical axis. (a) Perspex imager with reflective layer and additional lens. (b) Uncoated Perspex imager (without lens). The virtual image for the central rays lies in a more distant plane in this case.

already been used successfully for the reconstruction of the visual input of flying insects [19].

We thank F. Brink and the late G. Hunter at the Australian National University Electron Microscopy Unit, Research School of Biological Sciences, for vacuum deposition of the reflective layers. The work was supported by fellowships from the German Science Foundation (DFG) and the Centre for Visual Sciences (CVS) to W. Stürzl and N. Boeddeker. We acknowledge additional financial support from the Australian Research Council Centre of Excellence in Vision Science (J. Zeil and M. V. Srinivasan).

## References

1. M. Srinivasan, J. Chahl, K. Weber, S. Venkatesh, M. Nagle, and S. Zhang, "Robot navigation inspired by principles of insect vision," Robot. Auton. Syst. 26, 203–216 (1999).
2. M. Jogan and A. Leonardis, "Robust localization using panoramic view-based recognition," in *Proceedings of the 15th International Conference on Pattern Recognition* (IEEE, 2000), Vol. 4, pp. 136–139.
3. N. Winters, J. Gaspar, G. Lacey, and J. Santos-Victor, "Omnidirectional vision for robot navigation," in *Proceedings of the IEEE Workshop on Omnidirectional Vision* (IEEE, 2000), pp. 21–28.
4. A. Argyros, K. Bekris, S. Orphanoudakis, and L. Kavraki, "Robot homing by exploiting panoramic vision," Auton. Robot. 19, 7–25 (2005).
5. R. Möller, A. Vardy, S. Kreft, and S. Ruwisch, "Visual homing in environments with anisotropic landmark distribution," Auton. Robot. 23, 231–245 (2007).
6. Y. Onoe, N. Yokoya, K. Yamazawa, and H. Takemura, "Visual surveillance and monitoring system using an omnidirectional video camera," in *Proceedings of the Fourteenth International Conference on Pattern Recognition* (IEEE, 1998), Vol. 1, pp. 588–592.
7. G. Cielniak, M. Miladinovic, D. Hammarin, L. Goransson, A. Lilienthal, and T. Duckett, "Appearance-based tracking of persons with an omnidirectional vision sensor," in *Proceedings of the Fourth IEEE Workshop on Omnidirectional Vision* (IEEE, 2003).
8. T. E. Boult, X. Gao, R. Micheals, and M. Eckmann, "Omnidirectional visual surveillance," Image Vis. Comput. 22, 515–534 (2004).
9. J. Zeil, M. Hofmann, and J. Chahl, "Catchment areas of panoramic snapshots in outdoor scenes," J. Opt. Soc. Am. A 20, 450–469 (2003).
10. N. Boeddeker, J. Lindemann, M. Egelhaaf, and J. Zeil, "Responses of blowfly motion-sensitive neurons to reconstructed optic flow along outdoor flight plans," J. Comp. Physiol. A 191, 1143–1155 (2005).
11. W. Stürzl and J. Zeil, "Depth, contrast and view-based homing in outdoor scenes," Biol. Cybern. 96, 519–531 (2007).
12. J. Chahl and M. Srinivasan, "Reflective surfaces for panoramic imaging," Appl. Opt. 36, 8275–8285 (1997).
13. J. Chahl and M. Srinivasan, "Filtering and processing of panoramic images obtained using a camera and a wide-angle-imaging reflective surface," J. Opt. Soc. Am. A 17, 1172–1176 (2000).
14. R. Benosman, S. B. Kang, and O. Faugeras, eds., *Panoramic Vision: Sensors, Theory and Applications*, 1st ed. (Springer, 2001).
15. Panoramic Annular Lens—PAL360, http://www.tateyama.jp/product/p360/data_en/Images/catalog/pl.pdf.
16. S. Baker and S. Nayar, "Single viewpoint catadioptric cameras," in *Panoramic Vision*, R. Benosman, S. Kang, and O. Faugeras, eds. (Springer, 2001), pp. 39–70.
17. R. Swaminathan, M. Grossberg, and S. Nayar, "Caustics of catadioptric cameras," in *Proceedings of the Eighth IEEE International Conference on Computer Vision* (IEEE, 2001), Vol. 2, pp. 2–9.
18. W. Stürzl, H.-J. Dahmen, and H. Mallot, "The quality of catadioptric imaging—application to omnidirectional stereo," in *ECCV 2004*, T. Pajdla and J. Matas, eds. (Springer, 2004), Vol. 3021, pp. 614–627.
19. J. Zeil, N. Boeddeker, J. Hemmi, and W. Stürzl, "Going wild: toward an ecology of visual information processing," in *Invertebrate Neurobiology*, G. North and R. Greenspan, eds. (Cold Spring Harbor, 2007).